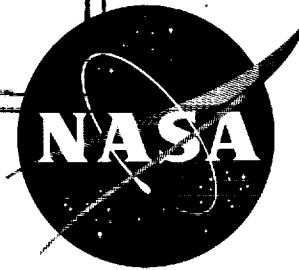


NASA TN D-1205

CASE FILE
COPY



TECHNICAL NOTE

D-1205

THE PERFORMANCE OF ABLATIVE MATERIALS IN A
HIGH-ENERGY, PARTIALLY DISSOCIATED,
FROZEN NITROGEN STREAM

By Nick S. Vojvodich

Ames Research Center
Moffett Field, Calif.

NATIONAL AERONAUTICS AND SPACE ADMINISTRATION
WASHINGTON

May 1962

2019-2020

2019-2020

2019-2020

2019-2020

2019-2020

2019-2020

2019-2020

2019-2020

NATIONAL AERONAUTICS AND SPACE ADMINISTRATION

TECHNICAL NOTE D-1205

THE PERFORMANCE OF ABLATIVE MATERIALS IN A
HIGH-ENERGY, PARTIALLY DISSOCIATED,
FROZEN NITROGEN STREAM

By Nick S. Vojvodich

SUMMARY

Tests of the organic ablative materials polyethylene, teflon, and nylon were conducted in a low-density, partially dissociated, frozen stream of arc-heated nitrogen to investigate the effect of surface catalysis on ablator performance. The facility duplicated the stagnation region heating rate to a body of 1-foot radius at an altitude of approximately 160,000 feet and at velocities between 11,500 and 22,000 feet per second.

The experimental variations of mass loss rate with stream energy agreed with the theoretical variations derived in the paper for a fully catalytic surface. This agreement indicated that no appreciable alteration in low-temperature ablator performance occurs when the vehicle operates in a nonequilibrium flight regime.

The mass loss rates when combined with measured heating rates gave effective heats of ablation which, for polyethylene and nylon, were lower than in previous data. The difference was due to the low heating rates of the tests (60 to 180 Btu/ft² sec) which caused a large percentage of the total ablated material to flow as liquid rather than be injected into the boundary layer more efficiently as vapor. It is shown that the stagnation-point ablation rate of full-scale liquid-layer ablators cannot be simulated by testing small-scale bodies, but a method is presented which allows their flight performance to be estimated.

INTRODUCTION

The ability of materials to provide adequate thermal protection for reentering vehicles by the ablation process has been studied in detail both theoretically (see, e.g., refs. 1 and 2) and experimentally (see, e.g., refs. 3, 4, and 5). In all cases both theory and experiment have been confined to a stream in chemical and thermodynamic equilibrium.

Recent work (see, e.g., refs. 6 and 7) has shown that for flight at high velocity and altitude (greater than 20,000 ft/sec and 200,000 ft, respectively), chemical reactions in the boundary layer are frozen and a sizable portion of the total heating rate consists of the heat of recombination that is released when the diffused atoms recombine on the surface. This process is controlled by surface catalysis and has been analyzed theoretically for a nonablating surface in reference 6, which showed that a considerable reduction in heating rate will exist for a noncatalytic surface.

Since much of a reentry flight will be in the high velocity and high altitude regime and since some vehicles are likely to be protected by ablative materials, the question arises as to the effect of ablator surface catalysis on total mass ablated. The purpose of this paper is to determine this effect. A study is also made to determine which aerodynamic parameters must be duplicated on a small-scale test body to simulate the stagnation-point ablation rate of a full-scale vehicle.

First, an analysis is made in which relationships describing the ablation and surface catalysis processes are combined. The analysis results in a prediction of mass loss rate which depends on surface catalytic efficiency as well as total enthalpy, impact pressure, and gasification factor, Γ . Experiments are then described in which three organic materials, nylon, polyethylene, and teflon, were ablated in an arc-heated, partially dissociated, frozen nitrogen stream at various energy levels. Their measurements are then compared to the theoretical values and to data from other high-energy facilities. Finally, the simulation parameters and the application of the data to flight are considered.

SYMBOLS

A	test sample surface area, ft ²
a	material viscosity constant, $\frac{\mu}{\mu_{\text{ref}}} = \exp\left(\frac{a}{T} - b\right)$, °R
c_p	specific heat, Btu/lb °F
\bar{c}_p	frozen specific heat of nitrogen gas, Btu/lb °F
D	diameter of test sample, ft
E	total stream energy, $\frac{V^2}{2gJ} + \bar{c}_p T + \alpha h_r$, Btu/lb
f_w	dimensionless mass injection rate, $\frac{-\rho_w V_w}{\sqrt{2 \frac{du_e}{dx} (\rho_e \mu_e)_s \left(\frac{\rho_w \mu_w}{\rho_e \mu_e}\right)^{0.2} g}}$

g	gravitational constant, ft/sec ²
H	specific enthalpy, $\frac{v^2}{2gJ} + \bar{c}_p T$, Btu/lb
H_{te}	stagnation point enthalpy at boundary-layer edge, $E = \bar{c}_p T_t + \alpha_e h_r$
h_f	latent heat of fusion, Btu/lb
h_r	heat of recombination of atoms, Btu/lb
h_v	latent heat of vaporization, Btu/lb
J	mechanical equivalent of heat, 778 ft-lb/Btu
k	thermal conductivity, Btu/sec ft °F
k_w	catalytic reaction rate constant, ft/sec
Le	Lewis number, Pr/Sc
M	molecular weight
m	mass of test specimen, lb
\dot{m}	total mass loss rate of ablation, lb/sec ft ²
\dot{m}_v	vapor mass loss rate, lb/sec ft ²
Nu	Nusselt number
P	power supplied to electrodes, kw
Pr	Prandtl number
p	pressure, lb/ft ²
Q^*	effective heat of ablation, Btu/lb
q	heat-transfer rate, Btu/ft ² sec
\bar{q}	dimensionless heat-transfer rate, $\frac{q}{\sqrt{2 \frac{du_e}{dx} (\rho_e \mu_e) \left(\frac{\rho_w \mu_w}{\rho_e \mu_e} \right)^{0.2}} g (H_{te} - H_w)}$
q_0	heat-transfer rate to nonablating surface, Btu/ft ² sec
R	nose radius, ft

Re	Reynolds number
Sc	Schmidt number
T	temperature, °R
T_m	melting temperature, °R
t	time, sec
u	x component of velocity, ft/sec
V	flight velocity, ft/sec
v	y component of velocity, ft/sec
\dot{w}	nitrogen mass flow rate, lb/sec
x	distance parallel to surface, ft
y	distance normal to surface, ft
α	mass fraction of atoms
β	$\frac{d\bar{q}}{df_w}$
Γ	gasification factor, $\frac{\dot{m}_V}{\dot{m}}$
ΔH	$H_{te} - H_w$, Btu/lb
ϵ	interface emissivity
η	efficiency
μ	viscosity, lb-sec/ft ²
ρ	density, lb/ft ³
σ	Stefan-Boltzmann constant, $\frac{5.08 \times 10^{-13} \text{ Btu}}{\text{ft}^2 \text{ } ^\circ\text{R}^4 \text{ sec}}$
τ	shear stress, lb/ft ²
ϕ	catalytic influence factor defined by equation (2)
Ω	liquid-layer parameter defined by equations (A4) and (A5)
ω	defined by equation (A3)

Subscripts

atm	atmosphere
av	average
e	outer edge of boundary layer
F	flight condition
i	gas-liquid interface
L	liquid layer
o	no mass injection
s	stagnation point
T	test condition
t	total
w	wall
ref	reference condition
1	condition ahead of shock wave
2	condition downstream of shock wave

ANALYSIS

In general, an ablative material when exposed to a high-energy gas stream first melts and upon further heating vaporizes. The energy absorbed in these phase changes, the reradiation from the hot surface, and the reduction of aerodynamic heating rate to the gas-liquid interface due to the injection of vaporized species into the boundary layer are the dissipation mechanisms of ablative materials.

The equation for the effective heat of ablation, which is the heat absorbed per pound of material ablated, can be obtained by the combination of the heat balance equation and the equation which gives the variation of interface heating rate with mass injection rate.

The steady-state heating to the gas-liquid interface is absorbed by the solid-liquid and liquid-gas phase changes and may be defined by the heat balance equation,

$$q = [\dot{m}(c_p T_m + h_f) + \dot{m}_v h_v] + \sigma \epsilon T_i^4 \quad (1)$$

For the low-temperature ablators considered in this investigation,

$$\sigma \epsilon T_i^4 \ll [\dot{m}(c_p T_m + h_f) + \dot{m}_v h_v]$$

and therefore will be neglected.

Chung, in reference 8, used similarity solutions of the set of conservation equations which describe the frozen boundary-layer flow of a viscous, compressible, partially dissociated diatomic gas to obtain the variation of the total heating rate q with mass injection rate at the stagnation point. The results were obtained for surfaces of various catalytic efficiencies at three values of the parameter α_{eh_r}/H_{te} , the ratio of the chemical energy to the total energy at the boundary-layer edge. It was assumed in this analysis that the boundary-layer reactions were chemically frozen, that the injected species did not react with the constituents already present in the boundary layer, and that the Lewis and Prandtl numbers had the constant values 1.4 and 0.71, respectively.

The results of reference 8 may be summarized as follows:

$$q = C_1 \sqrt{\frac{du_e}{dx}} (\rho_e \mu_e) \left(\frac{\rho_w \mu_w}{\rho_e \mu_e} \right)^{0.2} g (H_{te} - H_w) \left[1 + \frac{\alpha_{eh_r}}{H_{te}} (C_2 \varphi - 1) \right] \quad (2)$$

where

$$\varphi = \frac{1}{1 + \frac{C_3 \sqrt{\frac{du_e}{dx}} (\rho_e \mu_e) \left(\frac{\rho_w \mu_w}{\rho_e \mu_e} \right)^{0.2} g}{k_w \theta_w}}$$

The values of C_1 , C_2 , and C_3 which depend on the dimensionless mass injection rate f_w are

$-f_w$	C_1	C_2	C_3
0	0.827	1.251	1.033
.354	.462	1.375	1.135
.530	.295	1.499	1.193
.707	.140	1.969	1.248

The catalytic parameter ϕ is a function of the gas surface interface recombination rate k_w . If all the atoms that diffuse through the boundary layer to the interface recombine, $k_w = \infty$ and $\phi = 1$. However, when none of the incident atoms recombine, $k_w = 0$ and $\phi = 0$.

Variations of dimensionless heating rate \bar{q} with f_w at a particular value of α_{ehr}/H_{te} for values of ϕ between 0 and 1.0 are shown in figure 1. Since the curves are essentially linear for this range of f_w , the variation of \bar{q} with f_w may be expressed as

$$\bar{q}(\phi) = \bar{q}_0(\phi) + \left[\frac{d\bar{q}}{df_w}(\phi) \right] f_w \quad (3)$$

which may be rewritten

$$q(\phi) = q_0(\phi) - [\beta(\phi)] \dot{m}_v \Delta H \quad (4)$$

where

$$\beta(\phi) = \frac{d\bar{q}}{df_w} \quad \Delta H = H_{te} - H_w$$

Substitution of equation (4) into equation (1) yields the effective heat of ablation,

$$Q^* = \frac{q_0(\phi)}{\dot{m}} = (c_p T_m + h_f) + \frac{\dot{m}_v}{\dot{m}} [h_v + \beta(\phi) \Delta H] \quad (5)$$

Rearrangement of equation (5) yields

$$\dot{m} = \frac{q_0(\phi)}{(c_p T_m + h_f) + \Gamma [h_v + \beta(\phi) \Delta H]} \quad (6)$$

where

$$\Gamma = \dot{m}_v / \dot{m}$$

Equation (6) shows that the mass loss rate \dot{m} is directly proportional to the zero injection heating rate q_0 and decreases as the injection effectiveness increases. As shown in figure 1, the \bar{q} intercept, \bar{q}_0 , and slope of a constant ϕ line, β , both diminish as the surface catalytic parameter ϕ diminishes. To assess the over-all effect of ϕ upon \dot{m} , the ratio $\dot{m}(\phi)/\dot{m}(\phi=1)$ is obtained from equation (6) to yield

$$\frac{\dot{m}(\phi)}{\dot{m}(\phi=1)} = \left[\frac{q_0(\phi)}{q_0(\phi=1)} \right] \left\{ \frac{c_p T_m + h_f + \Gamma [h_v + \beta(\phi=1) \Delta H]}{c_p T_m + h_f + \Gamma [h_v + \beta(\phi) \Delta H]} \right\} \quad (7)$$

The variation of normalized mass loss rate with stream enthalpy was calculated from equation (7) for three typical low-temperature ablative materials: teflon which sublimates, and polyethylene and nylon both of which melt and then vaporize. First the variation of \bar{q} with f_w was calculated from equation (2) for $\phi = 0, 0.2, 0.4, 0.6, 0.8$, and 1.0 at various values of the parameter $\alpha_e h_r / H_{te}$ (see fig. 1 for $\alpha_e h_r / H_{te} = 0.70$).

Next, the mass fraction of dissociated nitrogen at the boundary-layer edge corresponding to the energy level H_{te} was calculated by means of Lighthill's relation (ref. 9) for the law of mass action in the form

$$\frac{\alpha_e^2}{1 - \alpha_e} = \frac{8.13}{\rho} \times 10^3 e^{-203,400/T} \quad (8)$$

where the density ρ and temperature T were obtained from a nitrogen Mollier chart with the assumption that the gas was nitrogen in dissociated equilibrium at an enthalpy H_{te} and a pressure of $1/3$ atmosphere.

Finally, the material properties $\beta(\phi=1)$ and the heat capacity $(c_p T_m + h_f + h_v)$ were obtained from the literature. The blowing parameter, $\beta(\phi=1)$, was taken as 0.44 for teflon (ref. 3) and 0.5 for polyethylene (ref. 10) and nylon (unpublished data of A. Chapman of Langley Research Center, NASA). The heat capacities $(c_p T_m + h_f + h_v)$, obtained from the same references, were 750 , 566 , and 1859 Btu/lb for teflon, nylon, and polyethylene, respectively. By measurements described in the next section, the gasification factor was determined to be 0.6 for polyethylene and nylon and 1 for teflon.

This information was then combined and substituted into equation (7) to yield the variation of normalized mass loss rate $\dot{m}(\phi)/\dot{m}(\phi=1)$ with stream enthalpy, shown plotted for each material in figure 2.

It is of interest to note that there is essentially no catalytic effect until H_{te} is equal to 3500 Btu/lb. This is because no dissociation has taken place and $\alpha_e = 0$. At higher values of enthalpy it is possible to obtain a considerable reduction in mass loss rate if the surface is noncatalytic ($\phi = 0$). For polyethylene, for example, this reduction is 30 percent at an enthalpy level of 8000 Btu/lb. As previously mentioned, both β and q_0 diminish as ϕ is reduced. The ratio $\dot{m}(\phi)/\dot{m}(\phi=1)$ is directly proportional to $q_0(\phi)$ and increases as $\beta(\phi)$ is diminished. (See eq. (7).) Therefore, the largest reduction in mass loss for a given material will occur when $\Gamma = 0$ since, for no blowing, the reduction in $q_0(\phi)$ is the only effect present.

EXPERIMENT

Test Apparatus

Tests were conducted in a high-energy low-density stream generated by an arc-jet wind tunnel. A nitrogen stream was heated by a d-c electric arc to energy levels between 2,000 and 10,000 Btu/lb. The resultant high-energy, partially dissociated gas was then expanded from a plenum chamber at a pressure of $1/3$ atmosphere through a contoured supersonic nozzle and discharged as a 4 -inch-diameter free jet at a Mach number of 5 into a vacuum chamber. The test chamber was evacuated to a static pressure of 200 microns of Mercury by a steam-jet ejector system. A schematic drawing of the test facility is presented in figure 3.

Test Specimens

The ablation test specimens were axisymmetric $1/2$ -inch-diameter cylinders with a nose radius of 0.537 inch and were machined of the organic materials nylon, teflon, and high-density polyethylene. The actual test sample was a 0.30-inch-diameter slug pressed into the concentric main body before the nose radius was turned. A dimensioned drawing of a typical test specimen is given in figure 4.

Test Procedure

The ablation specimens were tested in the following manner: A sting support holding eight test specimens equally spaced at 45° intervals, as shown in figure 3, was mounted in the vacuum chamber which was then pumped down. The arc was initiated between the electrodes, and, when steady flow conditions existed, a $3/4$ -inch-diameter shield was removed from in front of the test specimen which was located on the stream center line, 1 inch downstream of the nozzle exit. After the specimen was exposed to the heated stream for a predetermined time, the arc power was shut off, a new specimen was rotated into the stream, and the shield was replaced. This procedure was repeated until four specimens of the same material had been exposed to identical test conditions for various time intervals ranging between 5 and 20 seconds. After the runs, the test samples, which had been weighed on an analytical balance before the tests, were reweighed. Their weights were determined to 0.0004 gram. The runs were timed with a stopwatch which had a least count of 0.01 sec. This was done at various energy levels for polyethylene, teflon, and nylon specimens. In addition, both 16-mm motion pictures and 4×5 still pictures were taken of each specimen.

CONDITIONS OF TEST STREAM

Average State

The average stream energy was obtained from an energy balance. To determine all energy losses to the water-cooled parts, namely, the electrodes, plenum chamber, and nozzle, the water flow rates were visually observed on rotameters, and the incremental rise in water temperature T was sensed by chromel-alumel thermopiles and recorded on an oscillograph. The electrical power input, the product of arc voltage and arc current, was obtained from photographs of a precision ammeter and voltmeter. The net energy input to the gas was calculated from the formula

$$E_{av} = \frac{(P - \Sigma L)}{\dot{w}} 0.948$$

where ΣL is the sum of all energy losses to the water-cooled parts, P is the product of arc voltage and current, and \dot{w} is the nitrogen mass flow rate.

Center-Line State

Since the ablation measurements were made in the center of the 4-inch-diameter stream, the conditions there will now be discussed. The analysis and measurements reported in reference 11 indicated that stream energy, velocity, and impact pressure were relatively constant in the central core of the stream and diminished with increasing radius outside of the core. The size of the central core decreased with increasing energy and was 2 inches in diameter for the highest energy. Because of the uniformity of the stream properties in the central core, it was felt that calibration measurements on the stream center line would accurately define the test environment of the 1/2-inch-diameter ablation models. The energy of the gas on the center line was deduced from measurements of the stagnation-region heating rate and impact pressure on an axisymmetric bluff body. Plenum pressure was measured in order to define the chemical composition of the frozen stream. It will be recalled that the theory of reference 8, as summarized in equation (2), gives the variation of heating rate with stream energy for the case of chemically frozen boundary-layer flow, provided both the wall chemical activity and the degree of dissociation are known. Instruments for measuring the impact pressure and stagnation-point heating rate were located on the stream center line 1 inch downstream of the nozzle exit in order to obtain the energy of the test core at this axial position. The impact pressure at each value of total input energy was obtained with a 1/2-inch-diameter, water-cooled, impact pressure probe. Plenum chamber pressure was also measured and these two pressures

were sensed by a diaphragm-type strain-gage pressure cell which transmitted the signals to a recorder. The variation of impact pressure and plenum chamber pressure with total stream energy is plotted in figure 5.

The nonablating, transient-response, heat-transfer probe, shown in figure 6, consisted of a 0.300-inch-diameter, cylindrical, copper calorimeter supported in a stainless steel body by three 5 mil wires to minimize conduction losses. A chromel-alumel thermocouple junction was spot welded to the rear face of the calorimeter. The heat-transfer probe had external dimensions identical with those of the ablation specimens, with the exception of a 0.010-inch air insulation gap around the calorimeter, which was included to reduce heat loss to the stainless body. The temperature of the calorimeter was measured with the thermocouple junction on the rear face and was recorded as a function of time on an oscillograph by a high-sensitivity galvanometer in series with the thermocouple.

For the heat-transfer measurements the wall enthalpy of the calorimeter $H_w = \bar{c}_p T_w$ was small compared to the total enthalpy; consequently, the heating rate at a particular energy level $q \sim (H_{te} - H_w)$ was considered constant. Therefore, the initial slope of the temperature time record is a measure of the total heating rate experienced by the calorimeter and is given by the expression

$$q = \frac{mc_p}{A} \frac{dT}{dt}$$

(for negligible conduction and radiation losses).

The measurements of stagnation-point heating rate, which vary between 60 and 180 Btu/ft² sec, are plotted in figure 7 as a function of total input energy. These data exhibit considerable scatter partly because of the experimental technique requiring the inherently inaccurate measurement of a slope. Heating rates to a water-cooled probe of the same shape were determined from the mass flow and temperature rise of the cooling water and the data checked those obtained by the transient method. In order to assess the effect of stream ionization, the water-cooled probe was given a biasing voltage of ± 40 volts with respect to ground and no measurable difference in heating rate was observed. Subsequent studies of the attenuation of microwaves in the free stream have indicated that the ionization mass fraction is less than 0.1 percent.

The energy content of the nitrogen on the stream center line was obtained from the data in figure 7 in the following manner: Equation (2) for the heating rate may be expressed

$$q = q(H_{te}, \alpha_e, P_{t2}, \phi)$$

The catalytic parameter ϕ was assumed to be unity since the data of Linnett and Marsden (as reported by Goulard in ref. 12) show that copper has a high value of catalytic efficiency; thus

$$q = q(H_{te}, \alpha_e, p_{t_2})$$

Furthermore, the analysis and measurements of reference 11 show that the nitrogen mass fraction α remained constant as the stream flowed along the center line and through the shock wave; that is, $\partial\alpha/\partial y = 0$. Since H_{te} and p_{t_1} define the state of the gas in the plenum (i.e., ρ_{t_1} and T_{t_1}), α_e was computed from equation (8) in the form

$$\alpha_e = \alpha_e(p_{t_1}, H_{te})$$

Thus equations (2) and (8) may be combined to give

$$q = q(H_{te}, p_{t_1}, p_{t_2})$$

The measured values of impact pressure and plenum pressure were substituted into this expression to obtain the theoretical variation of heating rate with stream center-line energy shown as the solid line in figure 7. The measured heating rates, also plotted in figure 7, were then combined with this solution to yield the stream center-line energy at each test condition.

The variation of stream center-line energy with total input energy is plotted in figure 8. The solid line is fitted to the data points. The variation of average stream energy with total input energy is also plotted in figure 8. The slope of the upper curve (0.77) is the center-line efficiency and the slope of the lower curve (0.49) is the average efficiency. As described in reference 11, the flow of a high-energy, low-density stream is characterized by a thick boundary layer. The energy transferred from this hot boundary layer to the cooled nozzle wall results in a radial stream energy gradient. Thus, one would expect the trend indicated by the data of figure 8; that is, the energy of the gas at the center line of the stream is a maximum and much larger than the average energy. Since all ablation tests were made in the center of the stream, the variation of all measurements was plotted as a function of the center-line energy.

RESULTS AND DISCUSSION

Gasification Factor and Mass Loss

Figure 9 contains pictures of each material ablating at a stream center-line energy of 9500 Btu/lb. The second luminous region downstream of the test specimen is a result of the shock wave caused by the transverse portion of the model sting that spans a portion of the stream.

Figure 10 contains post-run pictures taken on an optical comparator of teflon, polyethylene, and nylon specimens, which were each exposed for 8 seconds at a stream center-line energy of 8050 Btu/lb. These have been superimposed upon the light gray pictures of the original unablated specimens, with dotted lines showing the original afterbody.

To obtain the gasification factor Γ for the two liquid-layer ablators, polyethylene and nylon, the runoff that solidified on the test specimen afterbody was removed and weighed, and its value was substituted into the following expression:

$$\Gamma = 1 - \left(\frac{A_{\text{sample}}}{A_{\text{specimen}}} \right) \left(\frac{m_{\text{runoff}}}{\Delta m} \right)$$

where A_{sample} and A_{specimen} are the surface areas of the test slug and ablation specimen, respectively. This equation was used to calculate Γ only for test specimens which had lost none of the liquid-layer runoff to the sting support. This technique yielded values of 0.6 for both materials. The distribution of the bubble formations on the nylon specimen shown in figure 10 indicated that the edge of the test sample may have promoted transition from a laminar to a turbulent boundary layer. Therefore, solid nylon models were tested at similar energy levels and no noticeable difference was observed between the surface condition of these models and those specimens containing inserts.

The reduction in mass Δm of each test specimen was plotted in figure 11 as a function of exposure time with stream center-line energy as a parameter. The slope of each line represents the mass loss per unit time \dot{m} for each energy level. This technique was employed to minimize the initial transient effects.

Effect of Surface Catalysis

The slope of each curve in figure 11 is plotted as a function of stream center-line energy in figure 12. Also plotted in figure 12 are the theoretical variations of mass loss rate \dot{m} with stream center-line energy for each material at $\phi = 1$ and 0. The fully catalytic curves ($\phi = 1$) were obtained by combining the measured heating rates to a catalytic surface q_0 (presented in fig. 7) with the values for the material properties measured in equilibrium flow facilities. The equation used was

$$\dot{m}(\phi=1) = \frac{q_0}{(c_p T_m + h_f) + \Gamma[h_v + \beta(\phi=1) \Delta H]} \quad (9)$$

The calorimeter heating rates were measured at a low surface temperature and hence must be multiplied by the factor $(H_{te} - 125/H_{te} - H_w)$ where H_w is the wall enthalpy of the ablator corresponding to its elevated temperature of operation and 125 is the enthalpy of the nitrogen at the calorimeter surface. The values of H_w (i.e., $\bar{c}_p T_w$) as well as other material properties are listed below

Material	$\beta(\phi=1)$	$H_w = \bar{c}_p T_w$, Btu/lb	h_v , Btu/lb	h_f , Btu/lb	Reference
Nylon	0.50	250	166	150	*
Polyethylene	.50	378	648	441	10
Teflon	.44	310	462	---	13

*Unpublished data of A. Chapman, Langley Research Center.

The experimentally determined Γ of 0.6 was used in equation (9) for polyethylene and nylon. The noncatalytic ($\phi = 0$) variation of mass loss rate with stream center-line energy was calculated from the relationship

$$\dot{m}(\phi=0) = \left[\frac{\dot{m}(\phi=0)}{\dot{m}(\phi=1)} \right] \dot{m}(\phi=1)$$

where the variation of the ratio $[\dot{m}(\phi=0)/\dot{m}(\phi=1)]$ is obtained from figure 2 for each material.

The coincidence of the experimental data with the $\phi = 1$ curves for all three materials indicates that for nylon, polyethylene, and teflon ϕ is close to unity. This may be attributed to a combination of the following two effects: The surface temperatures ($T_w \sim 1000^\circ \text{R}$) of these ablators are high enough that the values of the temperature-dependent parameter K_w (see ref. 12) for all three materials are close to those for catalytic metals. The collision cross sections of the injected species may be sufficiently large to make them efficient third bodies in promoting the recombination of nitrogen atoms near the gas-surface interface. Hence, it appears that the effectiveness of low temperature organic ablators is not severely altered when they operate in a nonequilibrium flight regime.

Effective Heats of Ablation

The effective heat of ablation was obtained by substituting the measured mass loss rates and hot wall heating rates into equation (5), $Q^* = q_o/\dot{m}$. The variation of Q^* with enthalpy potential for the three test materials studied in the low-density plasma-jet facility is presented

in figure 13 along with data from other high-energy test streams. The nominal test conditions of each facility, namely, stream energy, stagnation heating rates, and model exposure time are listed in the following table:

	Stream energy, E , Btu/lb	Heating rate, Btu/ft ² sec	Time, t , sec
NASA			
Langley			
Ethylene heated jet	1,200	100-125	20-40
Arc heated jet	3,000-8,000	2,000-3,500	8-15
Ames			
Low density plasma jet	3,200-9,500	60-170	4-20
Magnetically rotated arc jet	2,000	30-400	5-20
AVCO			
Arc jet	2,500-10,000	500-1,500	15

The solid lines of figure 13, labeled $\Gamma = 1$, are for equilibrium streams with heating rates high enough to fully vaporize the test materials. This condition existed for the teflon tests in both the Ames low-density plasma jet and AVCO arc-jet facilities. However, for the liquid-layer ablators, polyethylene and nylon, there is a sizable reduction in the effective heat of ablation because Γ was 0.6. To calculate the theoretical variation of the effective heats of ablation with enthalpy potential for nylon and polyethylene, the slope of the $\Gamma = 1$ curves, the material properties, and a value of 0.6 for Γ were substituted into equation (5). These are the solid curves labeled $\Gamma = 0.6$. The reduction in both the intercept and slope of these lines is due to the sub-unity value of 0.6 for the experimental Γ which, as explained in appendix A, is a result of the low heating rates at which these tests were conducted. It is interesting to note that the nylon and polyethylene data correlate well with the calculated curves for Γ of 0.6. In addition, the data point for nylon in the Langley ethylene heated stream (e.g., ref. 16) and the data points for polyethylene in the Ames magnetically rotated arc jet obtained at heating rates comparable to those of the presently reported tests also agree qualitatively with the data. The difference in heating rate between the Ames low-density plasma jet and the other facilities listed in the table is due primarily to the difference in impact pressure since the model scale and enthalpy potential of the facilities are comparable.

Simulated Flight Parameters

The stagnation-point convective heating rates to a body of 1-foot nose radius with the altitude-enthalpy history shown in figure 14 correspond exactly to the values measured with the test calorimeter. Also included in figure 14 is the nonequilibrium altitude zone, that defines

the state of the reactions in the boundary layer for this body with $T_w = 2700^\circ \text{R}$. For flight at this altitude the local Damkohler number (ratio of atom diffusion time to atom recombination time) is small enough to reduce the heating rate to a noncatalytic surface to 30 percent of the equilibrium value (ref. 6). For flight above this altitude the boundary-layer reactions become fully frozen and below this altitude they tend toward equilibrium because of the increase in density (ref. 7). The simulated trajectory lies above this transition zone and hence the plasma jet facility simulates the heating rates encountered in the nonequilibrium flight regime for full-scale bodies with $R \leq 1$ foot.

In order to apply the test ablation measurement to free flight of a full-scale vehicle, an analysis combining the liquid-layer and gas-layer equations is presented in appendix A to see which of the flight ablation parameters are simulated in the plasma jet tunnel. The performance of subliming ablators ($\Gamma = 1$), such as teflon, may be duplicated by simulating the stagnation enthalpy. However, the liquid-layer ablators, such as polyethylene and nylon, for which Γ is less than unity require the duplication of the gasification factor. This parameter depends upon the stagnation region shear stress gradient and heating rate as well as enthalpy. An approximate solution of the equations results in the relationship $\Gamma = \Gamma(\Omega)$ where Ω is a function of heating rate and enthalpy and is inversely proportional to the nose radius. The solution of this equation, plotted in figure 15, shows that the flight Γ is underestimated. In fact, a vehicle of 1-foot radius flying the simulated trajectory shown in figure 14 would have a value of Γ close to unity; the shear stress gradient acting on the small scale test body is unrealistically high. Therefore, the tests of small-scale bodies in a plasma jet tunnel fail to duplicate correctly the gasification factor because of the excessive shear stress gradient and also because the reentry deceleration forces, which tend to give a larger value of Γ , are not simulated.

SUMMARY OF RESULTS

An analysis has been presented which predicts the variation of the mass loss rate with surface catalytic efficiency for ablative materials in a nonequilibrium flight regime. It has been shown theoretically that a considerable reduction in mass loss rate may occur if the ablator surface is noncatalytic. For polyethylene, at 8000 Btu/lb, this reduction is 30 percent.

Mass loss rate for three materials, teflon, polyethylene, and nylon, was measured in a low-density, high-energy, partially dissociated, nitrogen stream at Mach number 5 to evaluate the effect of this nonequilibrium regime on ablative materials. The resulting variation of mass loss rate with enthalpy for each material when compared to theory shows that the

effectiveness of low-temperature organic ablative materials is not altered when the heating rate is due mostly to chemical recombination of atoms on the gas-liquid interface since they operated at temperatures which are high enough to make the surface catalytic.

Furthermore, it has been demonstrated that the experimental effective heat of ablation for liquid-layer ablators, such as polyethylene and nylon, is reduced severely when the small-scale test bodies are exposed to low heating rates.

Finally, an approximate solution of the liquid-layer conservation equations has been presented. The results indicate that in spite of correctly simulating heating rate and enthalpy at the stagnation point of a small-scale test, the measured ablation rate will be larger than may be expected on a full-scale vehicle because of the excessive shear-stress gradient which acts on the test body.

Ames Research Center
National Aeronautics and Space Administration
Moffett Field, Calif., Feb. 23, 1962

APPENDIX A

CAPABILITY OF ARC JET TO SIMULATE FLIGHT PARAMETERS

Before using ablation data obtained in an arc-jet test facility to predict the performance of an ablative heat shield on an actual flight vehicle, one must know how the pertinent aerodynamic parameters imposed on the small-scale test bodies compare to those on the full-scale vehicle. Since a subliming ablator loses its material in vapor form, it is necessary to duplicate only the stagnation enthalpy to obtain the correct effective heat of ablation (ref. 3). However, for a liquid-layer ablator, from equation (5) with ($\phi = 1.0$),

$$Q^* = \frac{q_0}{\dot{m}} = (c_p T_m + h_f) + \Gamma h_v + \Gamma \beta \Delta H \quad (A1)$$

Therefore, to duplicate the effective heat of ablation Q^* , the gasification factor, Γ , as well as H_{te} must be the same for both test body and flight vehicle. It is the purpose of this appendix to determine: (a) the pertinent aerodynamic parameters that control the gasification factor, and (b) to what extent these may be duplicated on a test body in an arc-jet facility.

GASIFICATION FACTOR

The steady-state surface ablation at the stagnation point was obtained by combining the liquid-layer energy, momentum, and continuity equations in the form (see ref. 4);

$$\dot{m} - \dot{m}_v = \frac{2\rho_L \bar{k}_L^2 T_i^2 (\partial \tau_i / \partial x)}{a^2 c_{pL}^2 \mu_{Li} \dot{m}^2} \quad (A2)$$

When equation (A2) is divided by \dot{m} and it is noted that $\dot{m}_v / \dot{m} = \Gamma$, the following equation is obtained

$$1 - \Gamma = \omega_L \left(\frac{T_i^2}{\mu_{Li}} \right) \frac{\partial \tau_i / \partial x}{\dot{m}^3} \quad (A3)$$

where

$$\omega_L = \frac{2\rho_L \bar{k}_L^2}{a^2 c_{pL}^2}$$

In equation (A1), for $\Delta H > 5000 \text{ Btu/lb}$

$$\Gamma \beta \Delta H \gg (c_p T_m + h_f) + \Gamma h_v$$

then

$$\frac{q_o}{\dot{m}} \approx \Gamma \beta \Delta H$$

Substitution of this into equation (A3) yields

$$1 - \Gamma \approx \left[\omega_L \left(\frac{T_1^2}{\mu_{L1}} \right) \frac{\partial \tau_o / \partial x}{q_o^3} (\beta \Delta H)^3 \right] \Gamma^3 \quad (A4)$$

where it can be shown that

$$\partial \tau_o / \partial x \approx \partial \tau_i / \partial x$$

and

$$1 - \Gamma \approx \Omega \Gamma^3 \quad (A5)$$

where Ω equals the bracketed quantity of equation (A4). The solution of this cubic $\Gamma = \Gamma(\Omega)$ is plotted in figure 15 and shows that Γ increases from 0.2 to 0.9 as Ω is decreased three orders of magnitude from 100 to 0.1. The parameters which appear in Ω may be grouped as follows:

$$\Omega = \left[\frac{T_1^2}{\mu_{L1} q_o^3} \right] \left[\frac{\partial \tau_o}{\partial x} \right] \left[(\Delta H)^3 \right] \left[\omega_L \right] \left[\beta \right]$$

The quantity ω_L is a function of liquid layer properties which will be the same on both test body and vehicle. The heating rate q_o determines the interface temperature which in turn controls viscosity. Therefore, if q_o is duplicated,

$$(T_1^2 / \mu_{L1} q_o^3)_T = (T_1^2 / \mu_{L1} q_o^3)_F$$

The blowing parameter β is determined essentially by the molecular weight of the injected species for $\phi = 1.0$; therefore, it will be considered a material property. Since the enthalpy potential is duplicated in the test stream, then Ω is proportional to the shear-stress gradient $\partial \tau_o / \partial x$. The gasification factor Γ is, in turn, related to the parameter Ω through equation (A5).

ENTHALPY AND HEATING RATE

For the range of flight velocities being considered here the radiation to the body from the dissociated species at the shock wave is small compared to the convective heating rate given by the laminar correlation of Fay and Riddell reported in reference 14; that is,

$$q_o = 4.9 \times 10^{-4} H_{te}^{1.075} \sqrt{\frac{p_{t2}}{R}} \quad (A6)$$

Since

$$(H_t)_F = (H_t)_T = V^2/2gJ \quad (A7)$$

the heating rate to the test body will be equal to that experienced by the full-scale vehicle when the ratio p_{t2}/R is the same for both bodies; that is,

$$(p_{t2}/R)_F = (p_{t2}/R)_T \quad (A8)$$

The flight impact pressure p_{t2} is related to the flight velocity and free-stream density by (see ref. 13)

$$(p_{t2})_F \approx \frac{(\rho_1)_F V^2}{g} \quad (A9)$$

Substitution of equation (A9) along with (A7), into (A8) yields

$$(\rho_1)_F = \left(\frac{R_F}{R_T} \right) \left(\frac{p_{t2}}{2H_{te}} \right)_T \frac{1}{J} \quad (A10)$$

Knowing the variation of the test body impact pressure with enthalpy, it is now possible to calculate from equation (A10) the heat-transfer simulated trajectory; that is, a body of nose radius R_F flying this density-enthalpy trajectory will experience convective heating rates which correspond to those on the full-scale body.

SHEAR-STRESS GRADIENT

The shear stress at the stagnation point of a nonablating surface may be related to the heating rate by means of Reynolds analogy, namely,

$$Nu = Re\tau_o/\rho_w u_e^2 \quad (A11)$$

Combining this with the correlation of reference 14 for the heating rate, that is,

$$q_o = \frac{Nu}{\sqrt{Re}} \sqrt{\rho_w \mu_w} \sqrt{\frac{du_e}{dx}} \frac{\Delta H}{Pr} \quad (A12)$$

yields the following expression for τ_o , ($Pr = 1$)

$$\tau_o \approx x \frac{q_o}{\Delta H} \frac{du_e}{dx} \frac{1}{g} \quad (A13)$$

The result of differentiating equation (A13) with respect to x is

$$\frac{\partial \tau_o}{\partial x} \approx \frac{q_o}{\Delta H} \frac{du_e}{dx} \frac{1}{g} \quad (A14)$$

Following reference 15 the stagnation-point velocity gradient is given as

$$\frac{du_e}{dx} \approx \frac{1}{R} \sqrt{\frac{p_{t2}}{\rho_{t2}}} \approx \frac{1}{R} \sqrt{\frac{H_{te} \mathbf{R} g}{\bar{c}_p}} \quad (A15)$$

where \mathbf{R} is the nitrogen gas constant equal to 55.2 ft-lb/lb $^{\circ}R$. Equations (A14) and (A15) are combined to give

$$\frac{\partial \tau_o}{\partial x} \approx \frac{q_o}{g \Delta H} \frac{1}{R} \sqrt{\frac{H_{te} \mathbf{R} g}{\bar{c}_p}} \approx \frac{q_o}{\sqrt{H_{te}}} \frac{1}{R} \sqrt{\frac{\mathbf{R}}{\bar{c}_p g}} \quad (A16)$$

The variation of Γ with altitude for flight of a body at a given speed may be estimated by combining equation (A16) and the expression for Ω which yield

$$\Omega \approx \left[\frac{1}{R} \sqrt{\frac{\mathbf{R}}{\bar{c}_p g}} (\Delta H)^{5/2} \frac{T_1^2}{\mu_{L1}} \omega_{L1} \beta \right] \frac{1}{q_o^2} \quad (A17)$$

where the bracketed quantity is a function of ΔH and material properties. Since the heating rate decreases with altitude, the performance of liquid-layer ablators will be decreased as the altitude increases (see fig. 15).

This qualitative explanation may also be applied to small-scale liquid-layer ablating bodies tested at the same enthalpy but at different heating rates. That is, from equation (A17), one would expect a decrease in the effective heat of ablation as the heating rate is decreased as a result of the reduction in Γ . The experimental measurements as well as the nylon data reported in reference 16 agree with this predicted trend.

If the full-scale heating rate and enthalpy have been successfully duplicated on the test model, equation (A16) will show that the ratio of shear-stress gradient on the model to full-scale value is inversely proportional to the nose radius ratio. Therefore, the viscous shear-stress gradient on the model will always be higher on the test body than on the full-scale vehicle unless, of course, full-scale test bodies are used. Hence, the flight gasification parameter Ω_F will always be smaller than Ω_T which, as shown in figure 15, results in a value of Γ_F greater than Γ_T .

On the basis of this analysis one may conclude that the tests of liquid-layer ablators conducted in an arc-jet facility with small-scale test bodies will underestimate the actual flight capability of these materials because of the excessive shear-stress gradient imposed on the test bodies.

REFERENCES

1. Scala, Sinclair M.: Sublimation in a Hypersonic Environment. Jour. Aero/Space Sci., vol. 27, no. 1, Jan. 1960, pp. 1-12.
2. Adams, Mac C.: Recent Advances in Ablation. ARS Jour., vol. 29, no. 9, Sept. 1959, pp. 625-632.
3. Georgiev, Steven: The Relative Merits of Various Test Facilities With Regard to Simulation of Hypersonic Ablation Phenomena. Proc. Hypervelocity Techniques Symposium, Denver, Colorado, Oct. 2, 1960, pp. 162-174.
4. Bowman, Gary H., and Savin, Raymond C.: An Experimental Investigation in an Atmosphere Entry Simulator of Nylon as an Ablative Material for Ballistic Missiles. NASA TM X-114, 1959.
5. Savin, Raymond C., Gloria, Hermilio R., and Dahms, Richard G.: Ablative Properties of Thermoplastics Under Conditions Simulating Atmosphere Entry of Ballistic Missiles. NASA TM X-397, 1960.
6. Goodwin, Glen, and Chung, Paul M.: Effects of Nonequilibrium Flows on Aerodynamic Heating During Entry Into the Earth's Atmosphere From Parabolic Orbits. Advances in Aeronautical Sciences, vol. 4; Proc. Second Inter. Cong. for Aeronautical Sciences, Pergamon Press, 1961, pp. 997-1018.
7. Grier, Norman T., and Sands, Norman: Regime of Frozen Boundary Layers in Stagnation Region of Blunt Reentry Bodies. NASA TN D-865, 1961.
8. Chung, Paul M.: Shielding Stagnation Surfaces of Finite Catalytic Activity by Air Injection in Hypersonic Flight. NASA TN D-27, 1959.
9. Lighthill, M. J.: Dynamics of a Dissociating Gas, Part I: Equilibrium Flow. Jour. Fluid Mech., vol. 2, pt. 1, Jan. 1957, pp. 1-32.
10. Wood, Robert M., and Tagliani, R. J.: Heat Protection by Ablation. Douglas Engineering Paper No. 813, Aug. 21, 1959.
11. Winkler, Ernest L., and Griffin, Roy N.: Effects of Surface Recombination on Heat Transfer to Bodies in a High Enthalpy Stream of Partially Dissociated Nitrogen. NASA TN D-1146, 1961.
12. Goulard, R.: On Catalytic Recombination Rates in Hypersonic Stagnation Heat Transfer. Jet Propulsion, vol. 28, no. 11, Nov. 1958, pp. 737-745. (Also: ARS Paper 544-57.)
13. Wentink, Tunis: High Temperature Behavior of Teflon. Res. Rep. 55, AVCO, Res. Lab., July 1959. (Air Force Ballistic Missile TN 59-15.)

14. Dedtra, R. W., and Hidalgo, H.: Generalized Heat Transfer Formulae and Graphs. AVCO Res. Rep. 72, March 1960.
15. John, R. R., and Bade, W. L.: Calibration of a Plasma Jet Facility for Simulation of Ballistic Missile Re-entry. AVCO RAD-TR-59-9, Feb. 20, 1959.
16. Bond, Aleck C., Rashis, Bernard, and Levin, L. Ross: Experimental Ablation Cooling. NACA RM L58E15a, 1958.

A
E
E
C
C

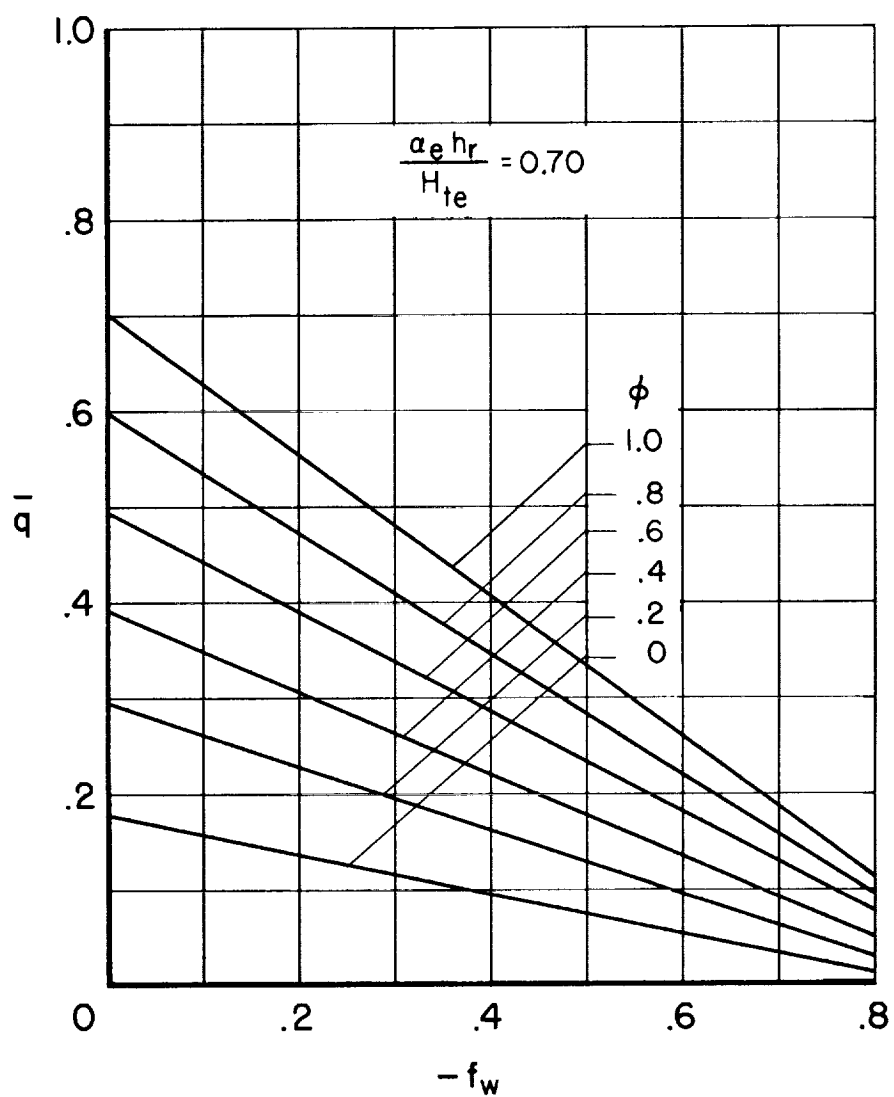


Figure 1.- Variation of dimensionless heating rate with mass injection parameter for various values of the catalytic parameter ϕ .

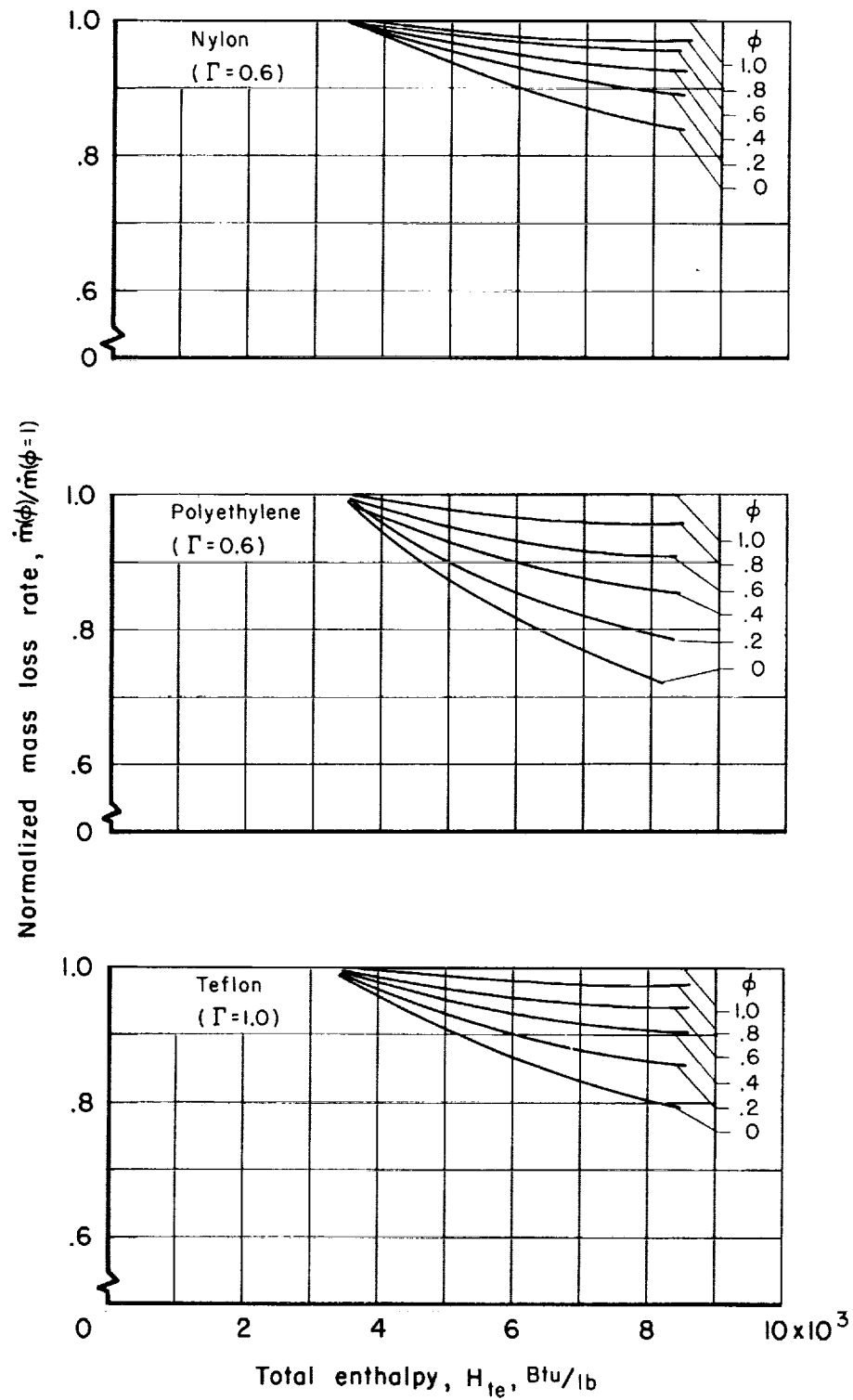


Figure 2.- Variation of normalized mass loss rate with total enthalpy at various values of the catalytic parameter ϕ .

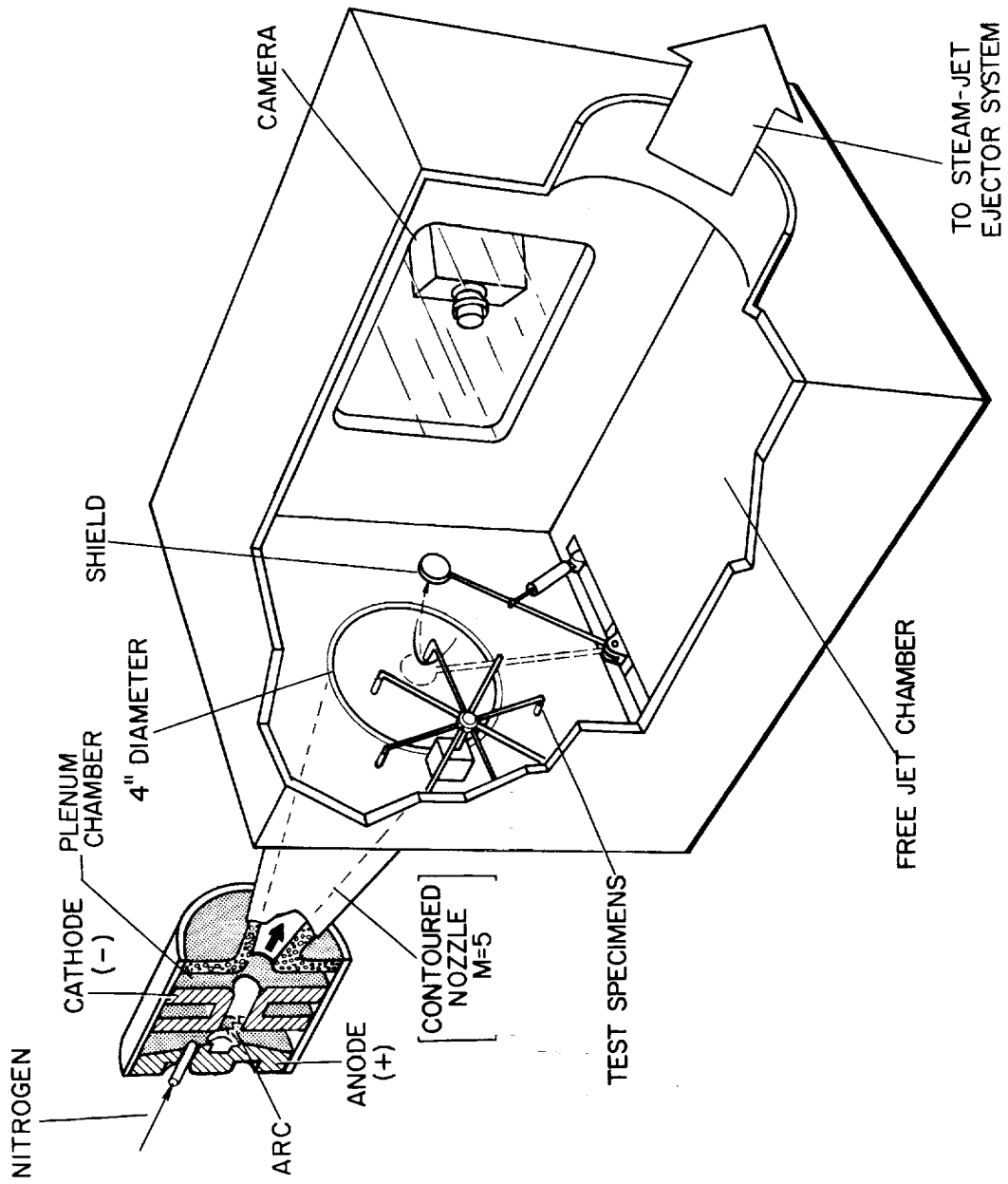
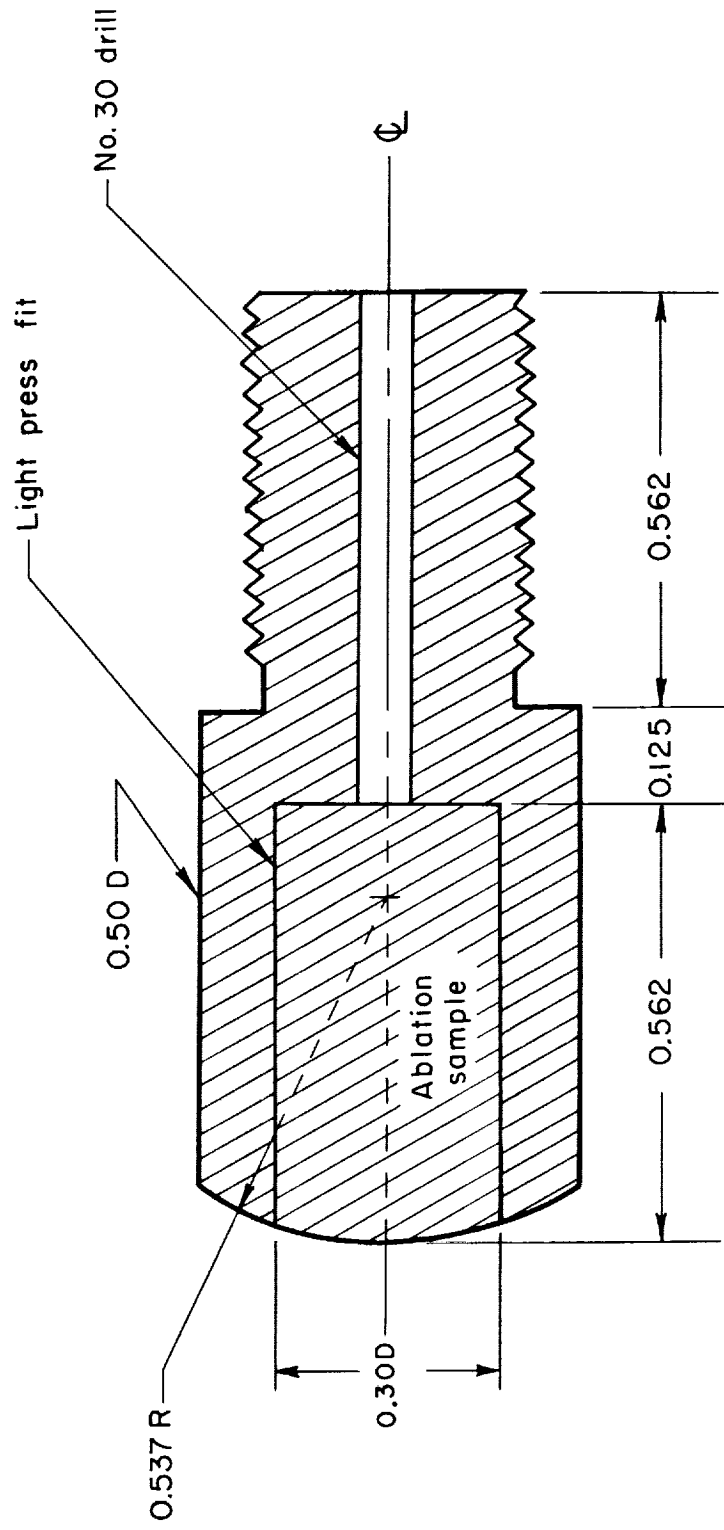


Figure 3.- Low-density plasma jet facility and experimental apparatus.



All dimensions in inches

Figure 4.- Ablation test specimen.

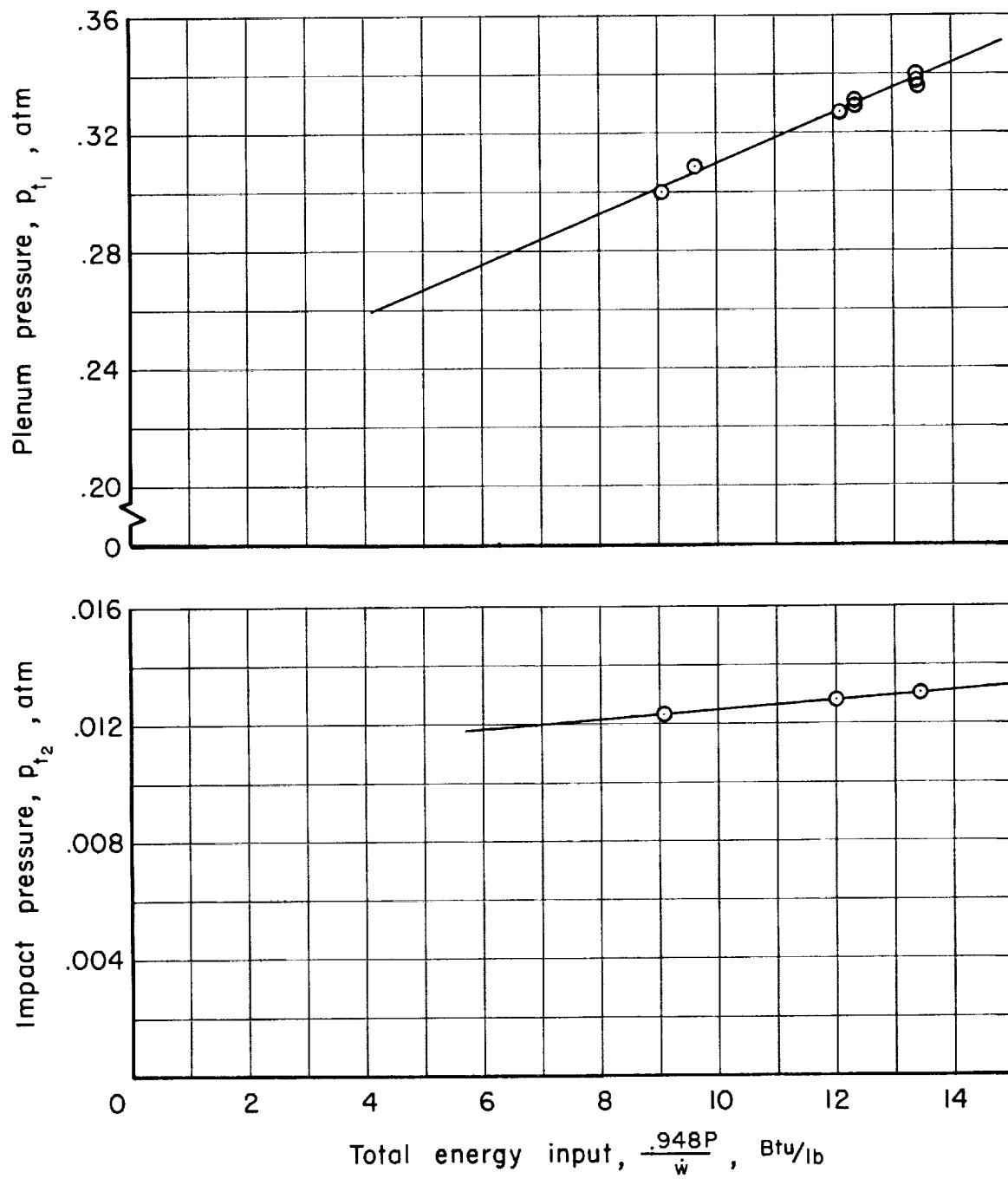


Figure 5.- Variation of impact and plenum pressure with total energy.

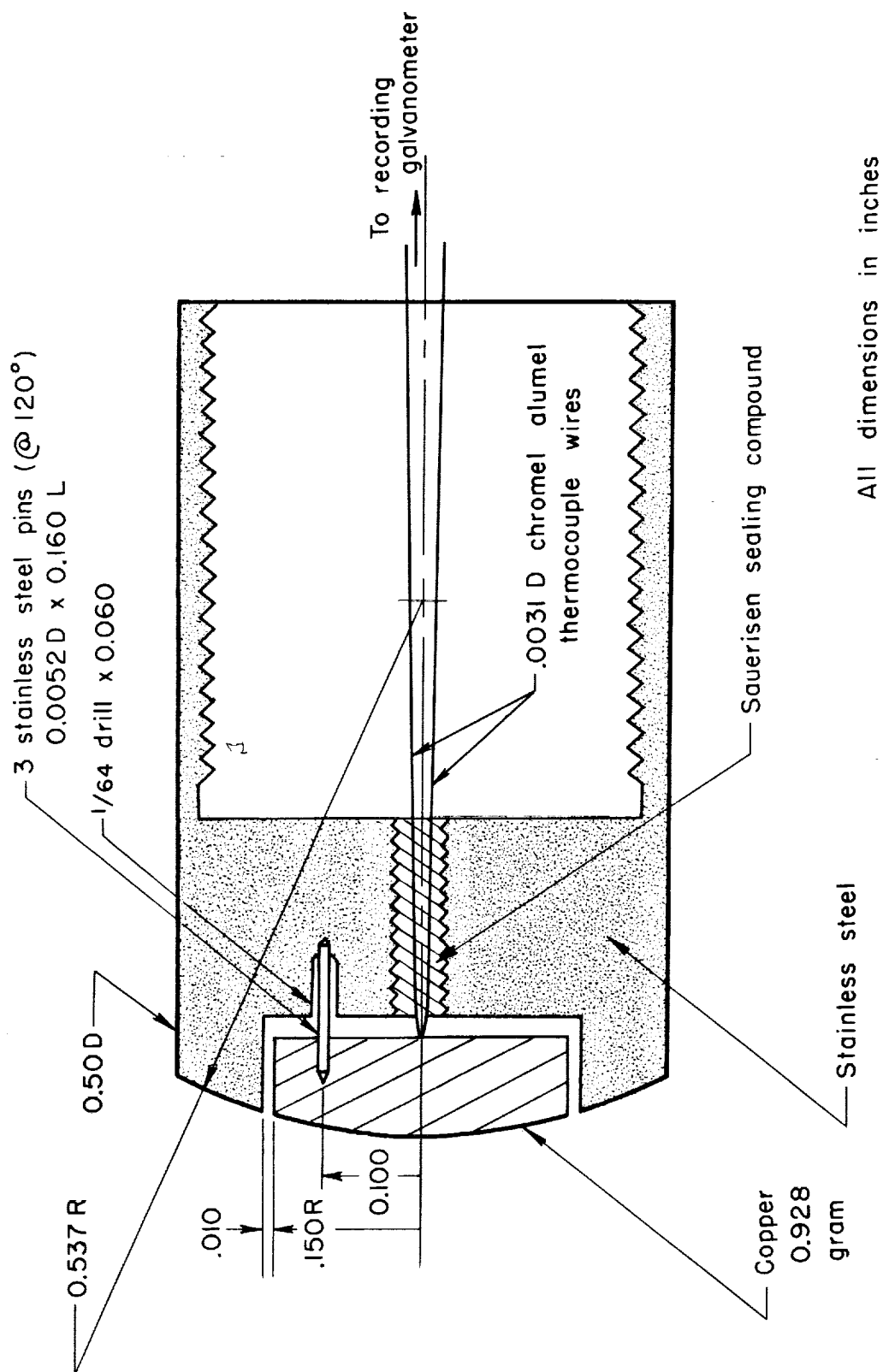


Figure 6.- Nonablating heat-transfer probe.

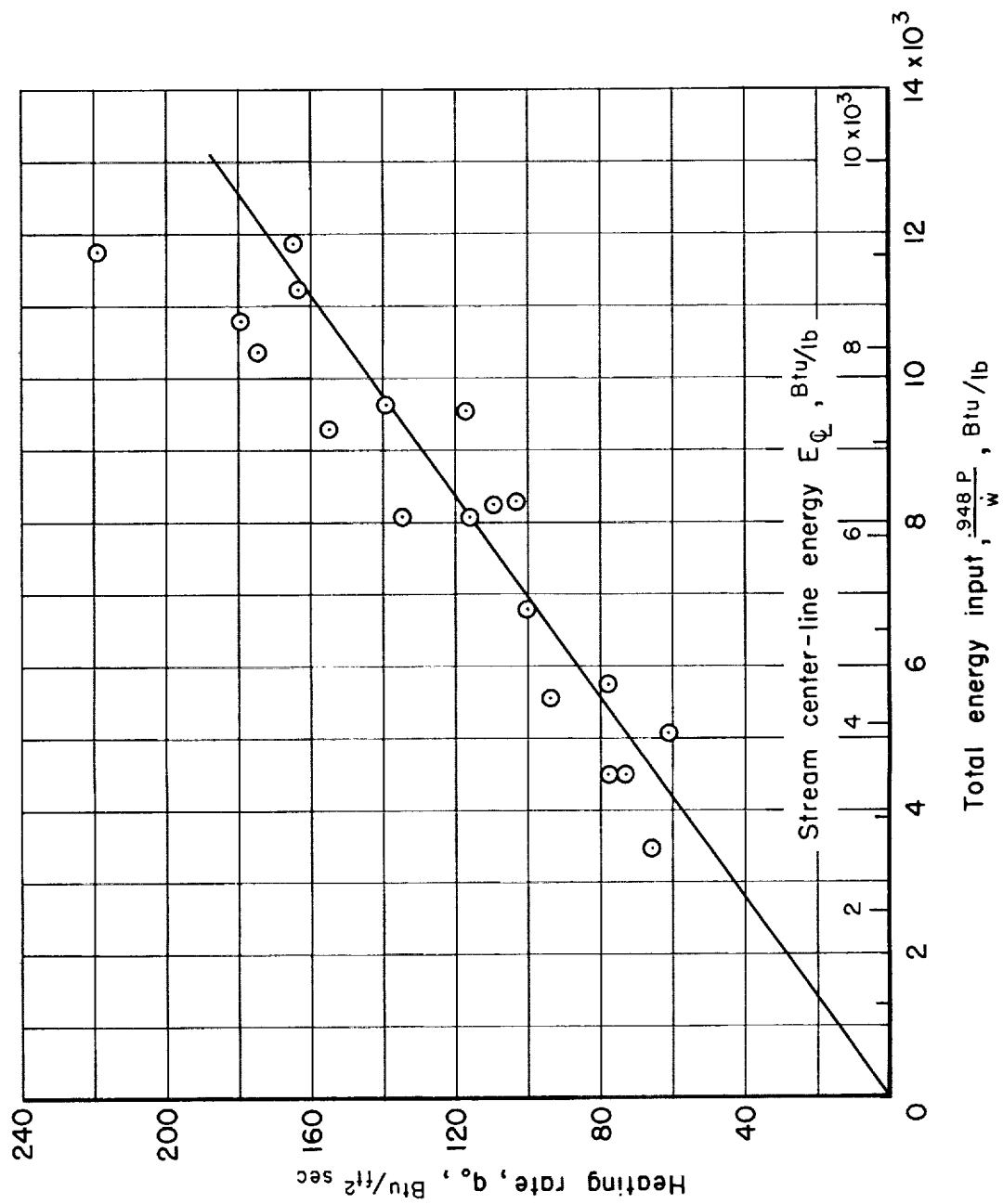


Figure 7.- Variation of nonablating heating rate with total energy input.

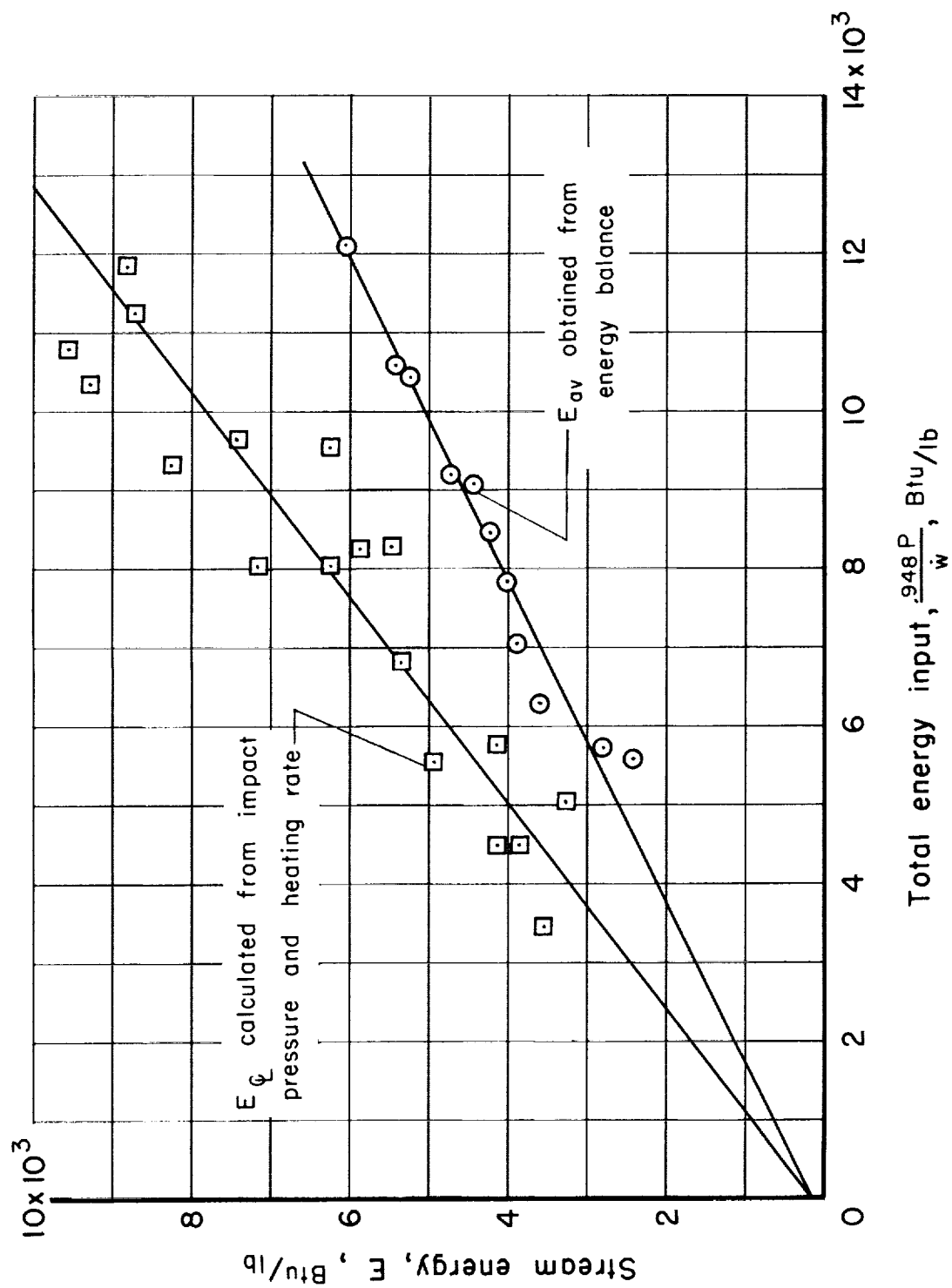


Figure 8.- Variation of center line and average stream energy with total input energy.

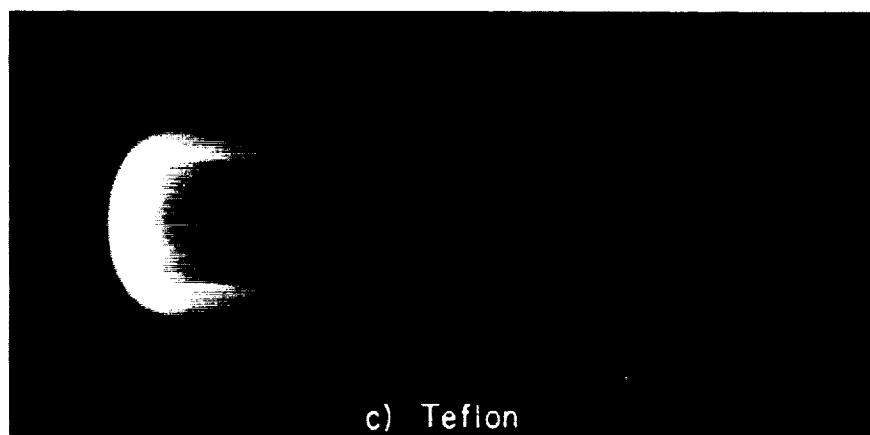
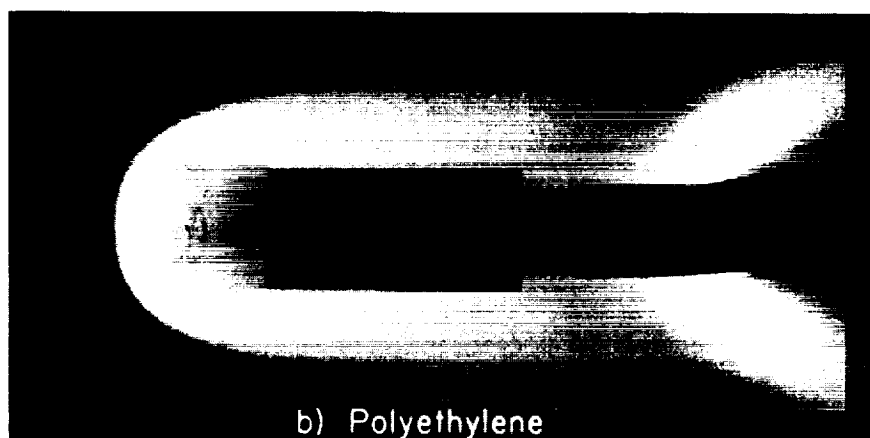
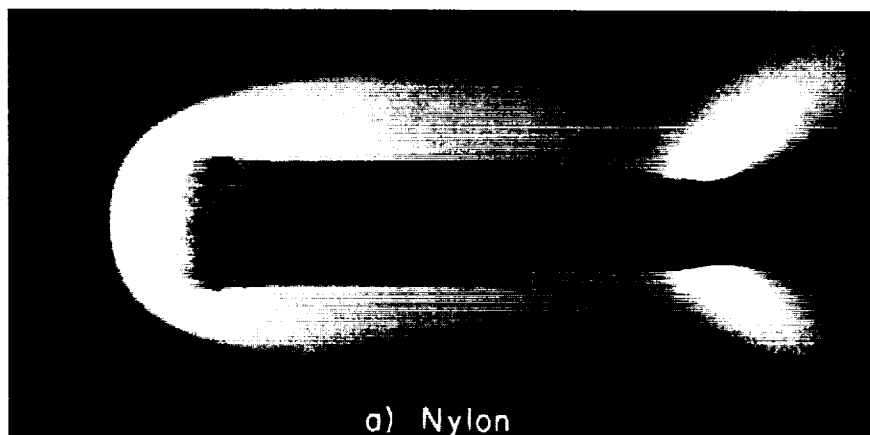


Figure 9.- Comparison of materials at stream energy of 9500 Btu/lb
for $t = 5$ sec.

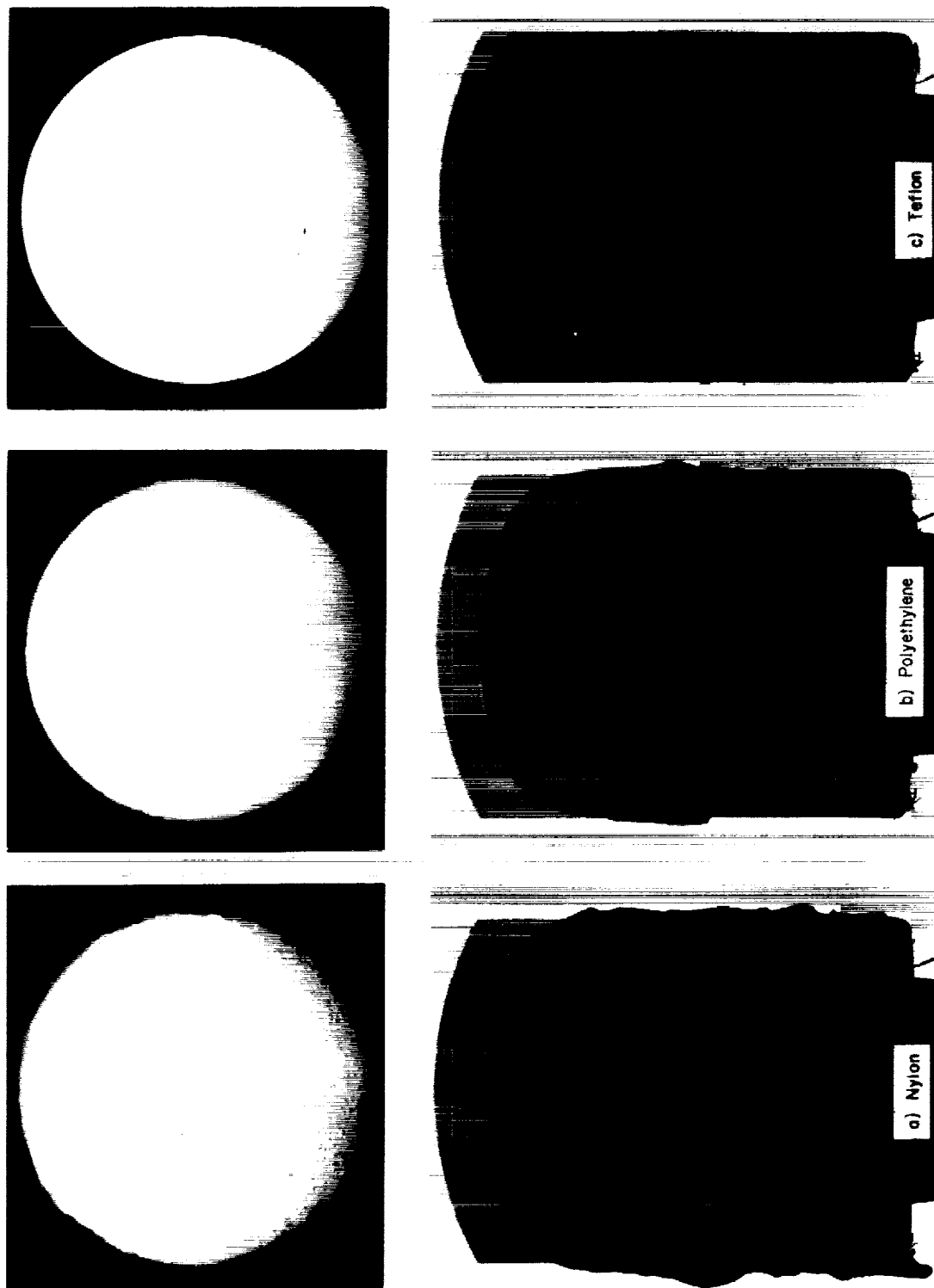


Figure 10.- Surface contour for each material tested at 8050 Btu/lb for 8 sec.

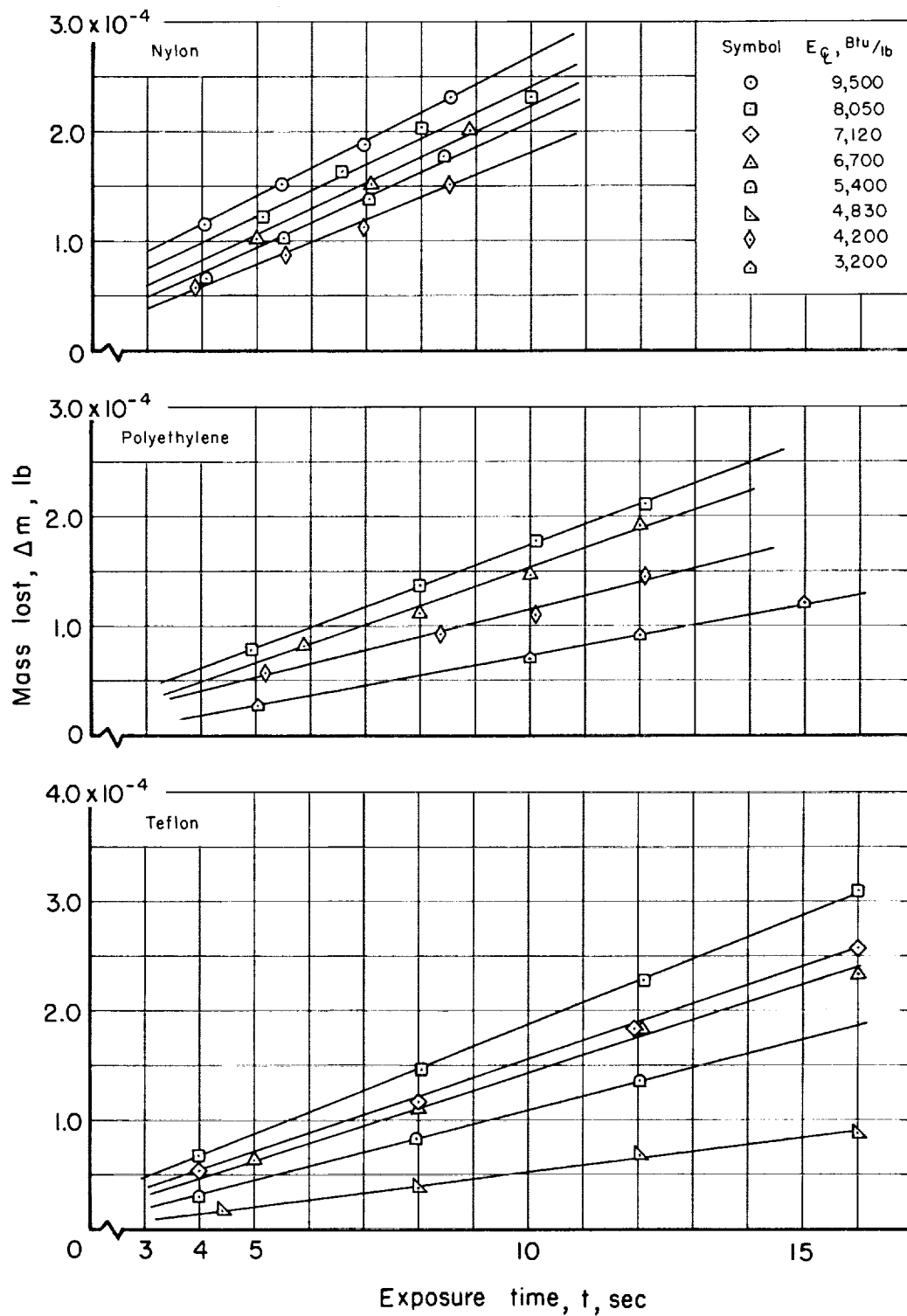


Figure 11.- Variation of mass loss with time at various stream center-line energies.

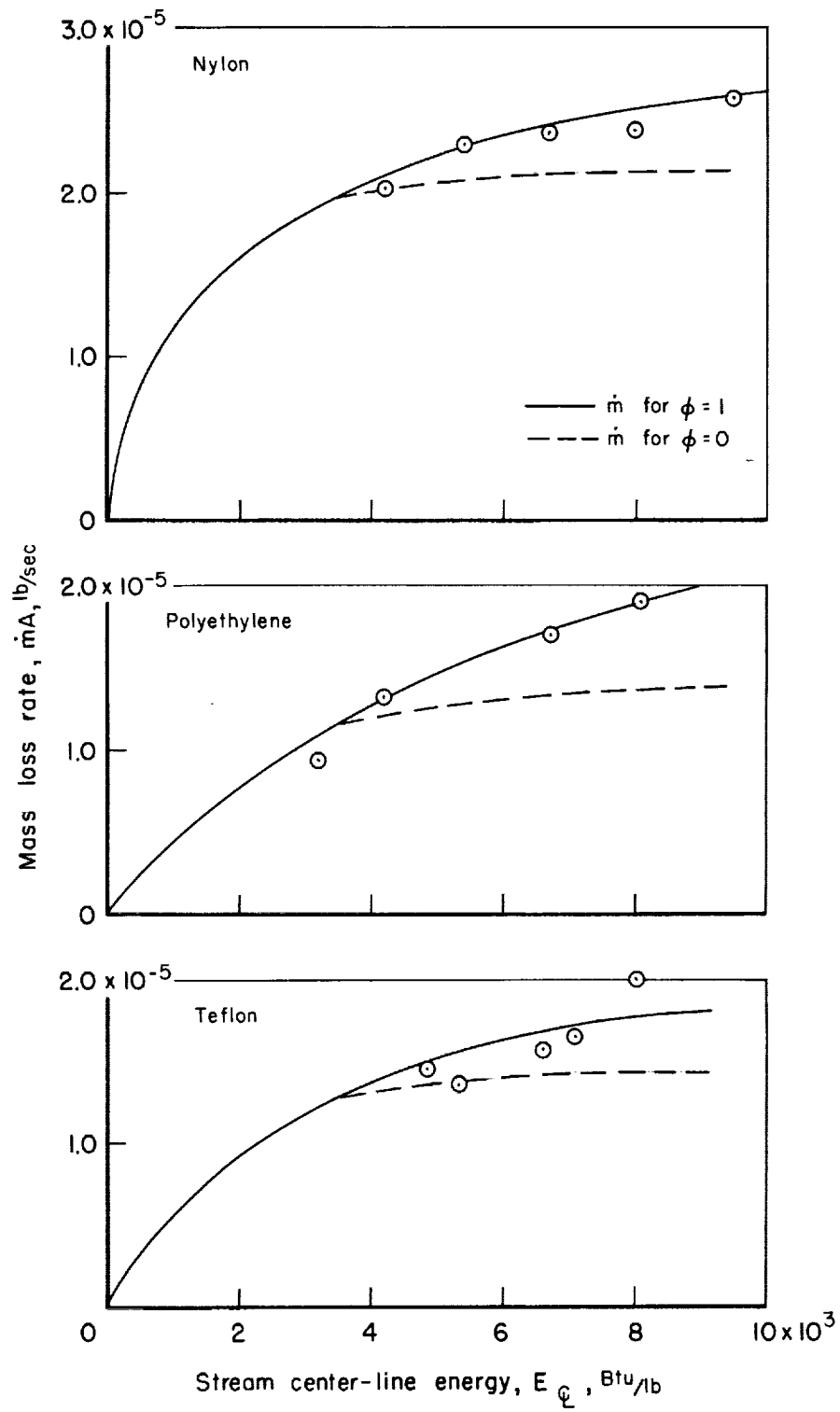


Figure 12.- Variation of mass loss rate with stream center-line energy.

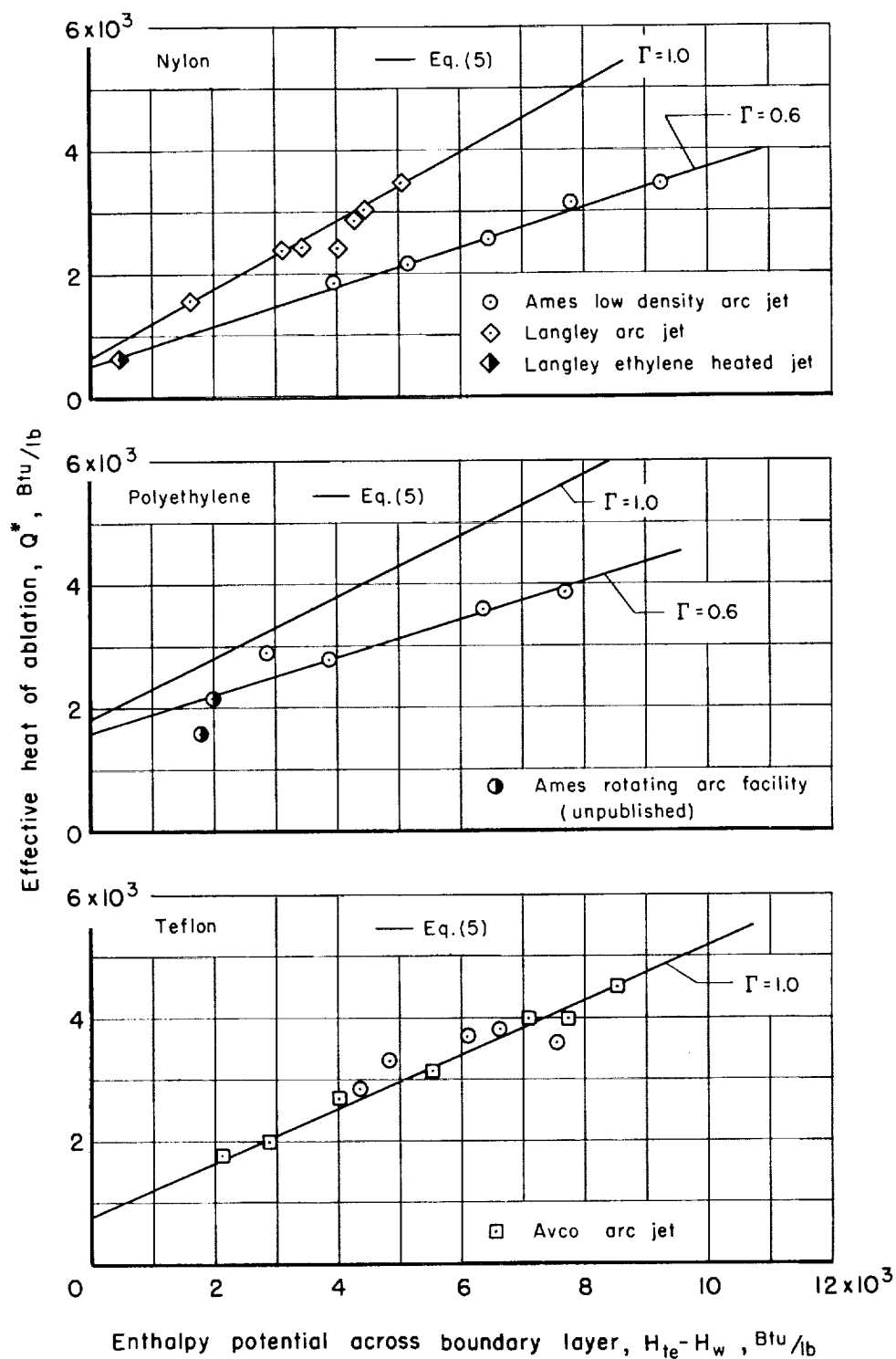


Figure 13.- Variation of the effective heat of ablation with enthalpy potential across the boundary layer.

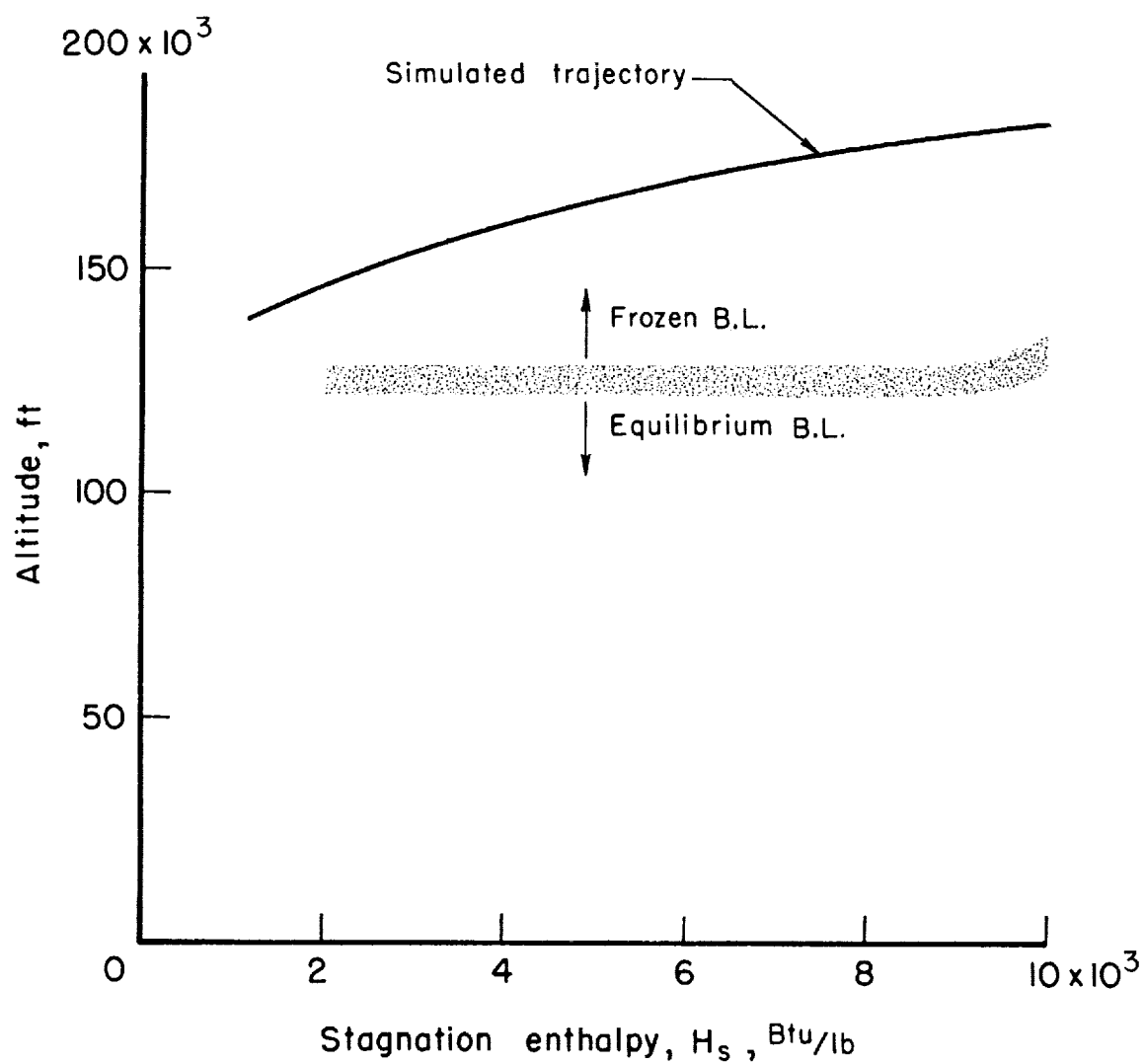


Figure 14.- Variation of altitude with stagnation enthalpy for simulated flight of a body of 1-foot radius.

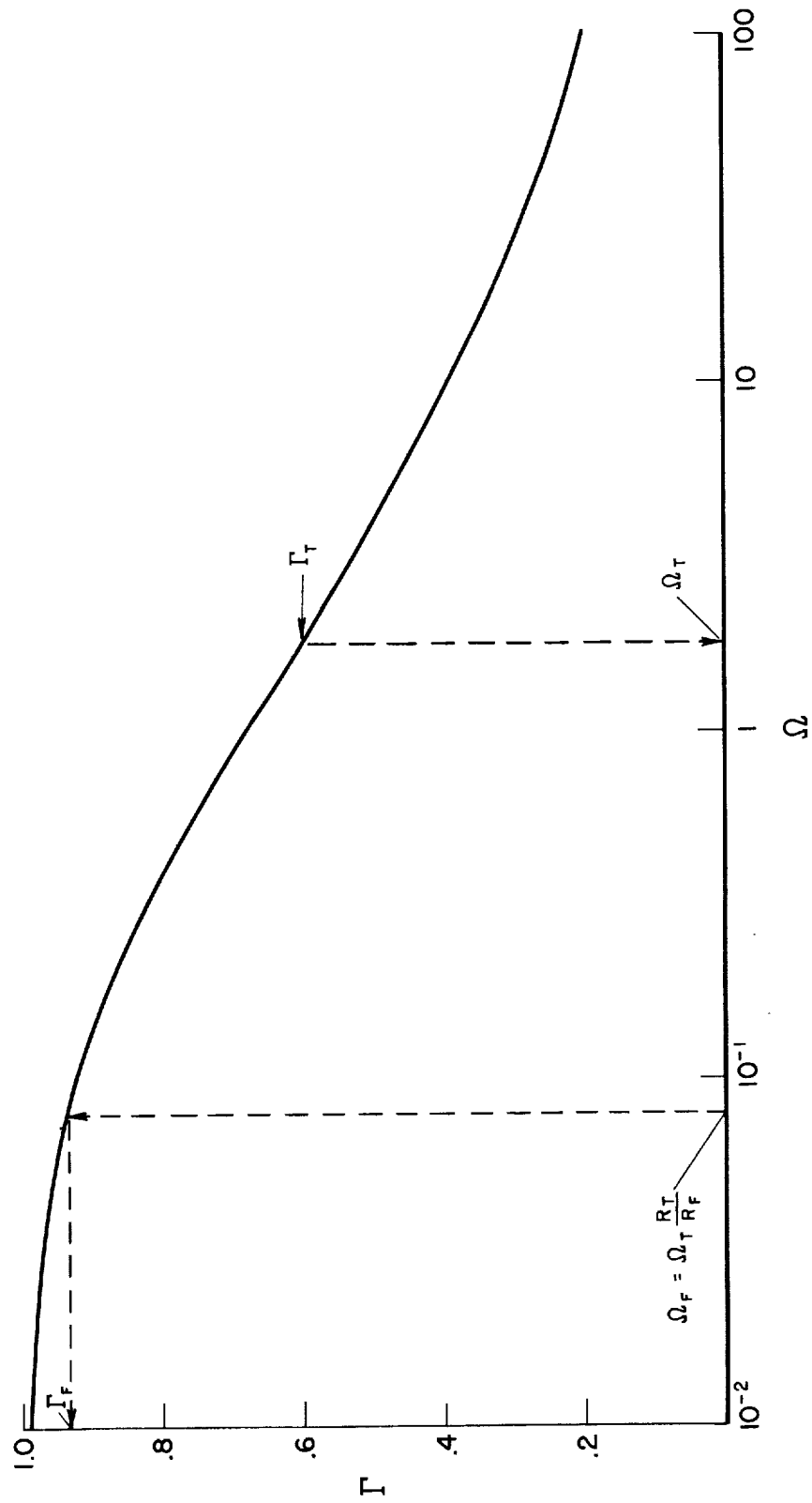


Figure 15.- Variation of gasification factor with liquid-layer parameter.

<p>NASA TN D-1205 National Aeronautics and Space Administration. THE PERFORMANCE OF ABLATIVE MATERIALS IN A HIGH-ENERGY, PARTIALLY DISSOCIATED, FROZEN NITROGEN STREAM. Nick S. Vojvodich. May 1962. 39p. OTS price, \$1.00. (NASA TECHNICAL NOTE D-1205)</p> <p>Tests of the organic ablative materials polyethylene, teflon, and nylon were conducted in a low-density, partially dissociated, frozen stream of arc-heated nitrogen to investigate the effect of surface catalysis on ablator performance. The facility duplicated the stagnation region heating rate to a body of 1 foot radius at an altitude of approximately 160,000 feet and at velocities between 11,500 and 22,000 feet per second. The experimental variations of mass loss rate with stream energy agreed with the theoretical variations derived in the paper for a fully catalytic surface. This agreement indicated no appreciable alteration in the performance of these low-temperature ablative materials in a nonequilibrium flight regime.</p>	<p>I. Vojvodich, Nick S. II. NASA TN D-1205</p> <p>(Initial NASA distribution: 14, Chemistry, organic; 20, Fluid mechanics; 25, Materials, engineering; 52, Structures.)</p> <p>NASA</p>	<p>NASA TN D-1205 National Aeronautics and Space Administration. THE PERFORMANCE OF ABLATIVE MATERIALS IN A HIGH-ENERGY, PARTIALLY DISSOCIATED, FROZEN NITROGEN STREAM. Nick S. Vojvodich. May 1962. 39p. OTS price, \$1.00. (NASA TECHNICAL NOTE D-1205)</p> <p>Tests of the organic ablative materials polyethylene, teflon, and nylon were conducted in a low-density, partially dissociated, frozen stream of arc-heated nitrogen to investigate the effect of surface catalysis on ablator performance. The facility duplicated the stagnation region heating rate to a body of 1 foot radius at an altitude of approximately 160,000 feet and at velocities between 11,500 and 22,000 feet per second. The experimental variations of mass loss rate with stream energy agreed with the theoretical variations derived in the paper for a fully catalytic surface. This agreement indicated no appreciable alteration in the performance of these low-temperature ablative materials in a nonequilibrium flight regime.</p> <p>NASA</p>	<p>I. Vojvodich, Nick S. II. NASA TN D-1205</p> <p>(Initial NASA distribution: 14, Chemistry, organic; 20, Fluid mechanics; 25, Materials, engineering; 52, Structures.)</p>
<p>NASA TN D-1205 National Aeronautics and Space Administration. THE PERFORMANCE OF ABLATIVE MATERIALS IN A HIGH-ENERGY, PARTIALLY DISSOCIATED, FROZEN NITROGEN STREAM. Nick S. Vojvodich. May 1962. 39p. OTS price, \$1.00. (NASA TECHNICAL NOTE D-1205)</p> <p>Tests of the organic ablative materials polyethylene, teflon, and nylon were conducted in a low-density, partially dissociated, frozen stream of arc-heated nitrogen to investigate the effect of surface catalysis on ablator performance. The facility duplicated the stagnation region heating rate to a body of 1 foot radius at an altitude of approximately 160,000 feet and at velocities between 11,500 and 22,000 feet per second. The experimental variations of mass loss rate with stream energy agreed with the theoretical variations derived in the paper for a fully catalytic surface. This agreement indicated no appreciable alteration in the performance of these low-temperature ablative materials in a nonequilibrium flight regime.</p>	<p>I. Vojvodich, Nick S. II. NASA TN D-1205</p> <p>(Initial NASA distribution: 14, Chemistry, organic; 20, Fluid mechanics; 25, Materials, engineering; 52, Structures.)</p> <p>NASA</p>	<p>NASA TN D-1205 National Aeronautics and Space Administration. THE PERFORMANCE OF ABLATIVE MATERIALS IN A HIGH-ENERGY, PARTIALLY DISSOCIATED, FROZEN NITROGEN STREAM. Nick S. Vojvodich. May 1962. 39p. OTS price, \$1.00. (NASA TECHNICAL NOTE D-1205)</p> <p>Tests of the organic ablative materials polyethylene, teflon, and nylon were conducted in a low-density, partially dissociated, frozen stream of arc-heated nitrogen to investigate the effect of surface catalysis on ablator performance. The facility duplicated the stagnation region heating rate to a body of 1 foot radius at an altitude of approximately 160,000 feet and at velocities between 11,500 and 22,000 feet per second. The experimental variations of mass loss rate with stream energy agreed with the theoretical variations derived in the paper for a fully catalytic surface. This agreement indicated no appreciable alteration in the performance of these low-temperature ablative materials in a nonequilibrium flight regime.</p> <p>NASA</p>	<p>I. Vojvodich, Nick S. II. NASA TN D-1205</p> <p>(Initial NASA distribution: 14, Chemistry, organic; 20, Fluid mechanics; 25, Materials, engineering; 52, Structures.)</p>

